Crystal structures and mechanical properties of superhard BC_2N and BC_4N alloys: First-principles calculations

Shiyou Chen and X. G. Gong
Surface Science Laboratory (National Key) and Physics Department, Fudan University, Shanghai 200433, China

Su-Huai Wei
National Renewable Energy Laboratory, Golden, Colorado 80401, USA

(Received 3 October 2007; published 31 January 2008)

Using first-principles calculation, we have investigated the structural and mechanical properties of the cubic (c)-BN/C_2 alloy systems, which are currently considered as strong candidates for superhard materials. We show that there is a sublinear dependence of the physical properties of the c-BC_2N alloy on the number of C–C and B–N bonds in the system. Structures that maximize the number of C–C and B–N bonds have low energy, high density, and high bulk and shear moduli. Structures with unstable B–B and N–N bonds are expected to have higher energy, lower density, and elastic moduli. Based on the "bond counting rule," we have identified a series of low-energy $(C_2)_n/(BN)_m$ (111) superlattices whose structural parameters are similar to the recently synthesized high-density BC_2N and BC_4N samples [Y. Zhao *et al.*, J. Mater. Res. **17**, 3139 (2002)]. The calculated bulk and shear moduli and ideal shear strengths under normal compression show that these BC_2N and BC_4N (111) superlattices are very strong in resistance to elastic distortion at equilibrium and plastic distortion under nanoindentation. Furthermore, we show that the calculated shear modulus and ideal shear strength under normal compression also have a sublinear relationship with the measured Vickers hardness for these high-density BN/C_2 alloy systems and could thus be used as a good indicator for the hardness of these alloys.

DOI: 10.1103/PhysRevB.77.014113 PACS number(s): 62.20.D−, 61.50.Ah, 61.50.Ks, 62.20.F−

I. INTRODUCTION

The design and synthesis of new superhard materials have recently drawn significant attention,[1–5] which is due to their wide range of industrial applications from cutting and polishing to protective coating. In the pursuit of superhard materials, the alloys of diamond and cubic (c)-BN, such as c-BC_2N and c-BC_4N,[4–7] have become one of the most promising candidates because they are expected to be thermally and chemically more stable than diamond and harder than c-BN.

Despite extensive studies carried out in the past few years, there are still many unresolved issues associated with the C_2/BN alloys, especially the origin of the scattered experimental data. Several groups have successfully synthesized BC_2N samples from a mechanical mixture of hexagonal BN and graphite (g) or g-BC_2N (Table I).[8–12] However, the measured physical properties of these samples are quite different. For example, the measured lattice constant of a c-BC_2N sample obtained by Knittle *et al.* using g-BN/graphite as the starting material is 3.602 ± 0.003 Å, about 0.3% larger than the ideal averaged lattice constant of diamond (3.567 Å) and c-BN (3.616 Å).[8] However, Solozhenko *et al.* synthesized c-BC_2N from g-BC_2N at high pressures and high temperatures,[10,13] and found that the measured lattice constant is 3.642 ± 0.002 Å, which is about 1.48% larger than the ideal value expected from Vegard's rule.[14] This is significantly larger than the values measured by other groups and even larger than that for c-BN. Their c-BC_2N samples also show some unusual physical properties, such as very small bulk modulus (259 ± 22 GPa) and shear modulus (238 ± 8 GPa), which are much smaller than those of c-BN and diamond (Table I), but the measured Vickers hardness (76 GPa) is higher than that of the c-BN single crystal (62 GPa).[10,13] More recently, Zhao *et al.* synthesized millimeter-sized bulk samples of superhard c-BC_2N and c-BC_4N using the mixture of graphite and g-BN as starting materials.[11] The x-ray diffraction peaks showed that BC_2N and BC_4N crystallize in the diamond-based cubic structure with lattice constants of 3.595 and 3.586 Å, respectively, which is only about 0.1% larger than the ideal average value and agrees well with the result of Utsumi *et al.*,[12] but much smaller than the value obtained by Solozhenko *et al.* for BC_2N.[10] The measured Vickers hardness is about 62 GPa for BC_2N and 68 GPa for BC_4N, much higher than that of c-BN (47 GPa) and second only to diamond (85 GPa).

Theoretically, various BC_2N structure models[6,7,15–18] have been proposed to understand the experimentally observed results. Sun *et al.*[18] searched all possible configurations of c-BC_2N within an eight-atom cubic diamond-based unit cell and identified seven topologically different structures of BC_2N-m ($m=1-7$). By calculating the lattice parameters and elastic constants using local density approximation (LDA) to the density functional theory, they showed that these structures could have either high density with high bulk and shear moduli or low density with low bulk and shear moduli, depending on the atomic configuration of C, B, and N. Recently, Kim *et al.*[19] performed calculations for some of the BC_2N-m structures using the general gradient approximation (GGA) to the density functional theory. Comparing to the LDA results, the GGA calculation gives large lattice constants and smaller bulk moduli.[20] Based on their calculated results, they argued that the two high-density structures, BC_2N-1 and BC_2N-2, correspond to the observed high-

 ©2008 The American Physical Society

TABLE I. The lattice constants a, bulk moduli B, and shear moduli G of diamond, c-BN, BC_2N, and BC_4N samples synthesized by different groups using different starting materials. Vickers hardnesses of diamond, c-BN, BC_2N, and BC_4N measured by two groups are also listed. Note that the values measured in Ref. 10 are systematically larger than the one obtained in Ref. 11.

Experiment	Structure	Starting material	a (Å)	B (GPa)	G (GPa)	H (GPa)	$H_{Diamond}$	$H_{c\text{-}BN}$ (GPa)
	Diamond		3.567[a,b]	443[a,c]	536[d]			
	c-BN		3.616[a,b]	369 ± 14[e]	414[f]			
Knittle *et al.*[a]	BC_2N	g-BN/graphite	3.602(3)					
Utsumi *et al.*[g]	BC_2N		3.595					
Solozhenko *et al.*[h]	BC_2N	g-BC_2N	3.642(2)	259 ± 22[i]	238 ± 8[i]	76	115	62
Zhao *et al.*[b]	BC_2N	g-BN/graphite	3.595(7)			62	85	47
Zhao *et al.*[b]	BC_4N	g-BN/graphite	3.586(9)			68	85	47

[a]Reference 8.
[b]Reference 11.
[c]Reference 18.
[d]Reference 30.
[e]Reference 31.
[f]Reference 32.
[g]Reference 12.
[h]Reference 10.
[i]Reference 33.

density structures by Utsumi *et al.*[12] and Zhao *et al.*,[11] whereas the relatively low-density BC_2N-3 structure corresponds to the low-density structure observed by Solozhenko *et al.*[10] because their calculated GGA lattice constants and bulk moduli are now closer to experimental values. They also suggested that BC_2N-m (m=4–7), which contain the high-energy B–B and N–N bonds, do not exist in the experimental samples and that the high-density phases are characterized by the existence of the C–C bonds, whereas the low-density phase is characterized by the absence of the C–C bond. A similar study was carried out by Zhou *et al.*,[22] who identified a tetragonal 16-atom structure with lower energy and higher density relative to BC_2N-1, and considered it as the most likely phase of the sample produced by Solozhenko *et al.*[10] However, due to the uncertainty in the LDA and GGA calculations,[20,21] it is not clear whether a direct comparison between the calculated structural parameters and the experimental data is a valid approach to distinguish experimental structures.

Recently, Zhang *et al.*[23] found that the calculated ideal strengths (the minimum stress that causes the breakdown of the crystal) of the seven BC_2N-m structures are all lower than that of c-BN; thus, they claimed that the hardness of the *optimal* BC_2N structure is lower than that of c-BN. They further claimed that the measured extreme hardness[10,11] of BC_2N nanocomposites is due to the nanocrystalline size effect and the bonding to the surrounding amorphous carbon matrix. Later, Pan *et al.*[24] modified their conclusion and proposed that the high-energy, low-density structure, BC_2N-5, with broken N–N bonds and very low ideal strength[23] can explain the extreme hardness of c-BC_2N observed in Ref. 10 because the shear strength can increase drastically if a compressive stress is applied along the N–N bond direction to cause a rebonding of the N–N bond. In this case, they used strength in a particular direction to infer the hardness. However, it is difficult to understand why all the nanocomposites can line up in an amorphous carbon matrix and behave as a single crystal.[10,23]

In a previous study, we have pointed out that a cubic BC_2N structure just means that the underlying lattice has the diamond $Fd\bar{3}m$ space group.[25–27] Because the alloys are usually synthesized under high temperature and high pressure conditions,[8–12] different ordered or disordered superstructures can form during growth, depending on the different methods and starting materials used in the synthesis. Therefore, limiting the theoretical study to certain cells such as the seven BC_2N-m structures[18,19] is not justified. By performing an unconstrained search, we have identified a series of low-energy, small-cell c-BN/C_2 alloys, which are c-BN/C_2 (111) superlattices (denoted as $BC_2N_{n\times n}$, with n=1, 2, 3, etc.).[25] These superlattices are energetically much more stable than any of the BC_2N-m superstructures.[18,23] They are also slightly more stable (about 2 meV per atom) than the proposed wurtzite ($n\times n$) BC_2N superlattices,[28,29] which is consistent with the fact that c-BN and diamond are more stable than wurtzite BN and lonsdaleite.[21] By calculating the ideal strength,[23,25] we found that these low-energy structures have higher ideal strength compared to c-BN; therefore, it is consistent with experimental observations[11] that c-BC_2N is harder than c-BN. We further point out that the (200) x-ray diffraction line is always weak for all the BN/C_2 alloys, which is due to the small differences among the atomic numbers of B, C, and N.[25]

To clarify the situation and understand the general chemical trend of the structural and mechanical properties of the c-BN/C_2 alloy systems, in this paper, we calculate the alloy formation energies, lattice constants, and bulk and shear moduli for a series of c-BC_2N structures with different bond components. We find that there is a sublinear dependence of physical properties of c-BC_2N on the bond components. Structures with more C–C and B–N bonds have low energy, high density, and high bulk and shear moduli, whereas those with B–B and N–N bonds have higher energy, lower density, and elastic moduli. These results validates the "bond counting rule," which is used to do the structural search. The systematic LDA errors for the lattice constants and bulk moduli

are corrected in a way that the calculated results can now be directly compared with available experimental data. Among the investigated structures, the low-energy $BC_2N_{n\times n}$ (111) superlattices have lattice constants closest to the values of the high-density sample measured by Zhao *et al.*,[11] indicating the possible existence of these superlattices in the synthesized samples. By calculating the shear moduli and ideal shear strength under normal compression for the BC_2N and BC_4N (111) superlattices, we find that these superlattices are strong in resistance to elastic distortion at equilibrium and plastic distortion under nanoindentation. Furthermore, we find that both the calculated shear moduli and ideal shear strength under normal compression have an almost linear relationship with the measured Vickers hardness[11] for diamond, *c*-BN, and the high-density BC_4N and BC_2N structures; thus, they could be used as an indicator for the hardness of these alloys.

II. CALCULATION METHODS

The total-energy and stress calculations for this study are carried out using density functional theory as implemented in the ABINIT code[34,35] that is based on pseudopotential and plane wave basis functions. The norm-conserving Troullier-Martins pseudopotential[36] is used with the cutoff radii of 1.59, 1.49, and 1.50 a.u. for B, C, and N, respectively. We use the LDA and the exchange-correlation functional of Perdew-Wang as parametrized by Goedecher *et al.*[37] For the Brillouin-zone integration, we used an $8\times8\times8$ Monkhorst-Pack *k*-point grid for an eight-atom cubic unit cell and equivalent *k* points for other structures.[38] The cutoff energy for the basis function is 80 Ry. Our convergence test of *k* points and energy cutoff shows that the uncertainty in the calculated stress values is less than 0.1 GPa.

The ideal tensile and shear strength is calculated using the standard approach as described in the literature.[39–41] To calculate the tensile stress, e.g., along the ⟨111⟩ direction of diamond, we construct a unit cell with one lattice vector along the ⟨111⟩ direction and the other two basis vectors perpendicular to the ⟨111⟩ direction. Then, we apply a small strain in the ⟨111⟩ direction and conduct the structural optimization for the lattice vectors perpendicular to the ⟨111⟩ direction and all the internal atomic positions.[42] The minimization is done until all the orthogonal components of the stress tensor are less than 0.1 GPa. For large stresses, the strain is increased step by step; at each step, the relaxed structure from the previous step is used as the starting point. We have compared the Hellmann-Feynman stress directly calculated in the ABINIT code and the one calculated by taking a derivative of the energy with respect to the strain[39–41] and have found that they agree. The shear stress and shear stress under normal compression[24] are computed in a similar way. Here, we first set the desired component of the target stress to be a certain value and all the other components to be zero. After finding the relaxed structure with the given stress, we increase the desired stress step by step. If a 0.5 GPa increase in the shear stress makes the structure collapse, we take that maximum shear stress as the shear strength along that direction.

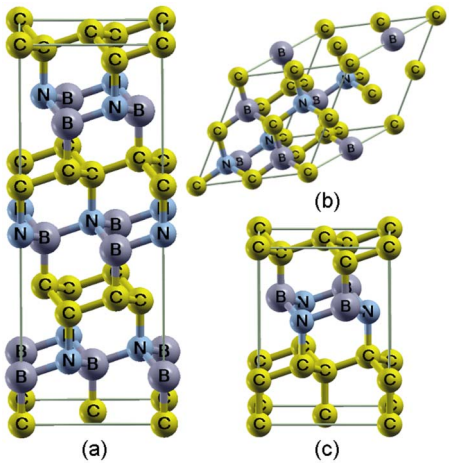

FIG. 1. (Color online) Crystal structures of (a) $BC_2N_{1\times1}$, $(C_2)/(BN)$ 1×1 (111) superlattice, (b) *r*-BC_2N, a 16-atom unit cell structure with eight C–C and B–N bonds per cell, and (c) $BC_4N_{2\times1}$, $(C_2)/(BN)$ 2×1 (111) superlattice.

III. RESULTS AND DISCUSSION

A. Crystal structures, bond-type parameter, and bond counting rule

Unlike for an isovalent semiconductor alloy in which the bond type is uniquely determined by its concentration, for nonisovalent alloys such as BC_2N, the type of bonds in the alloy is not determined by the alloy concentration ($x=0.5$). Depending on the occupation of B, N, and C atoms on the underlying diamond lattice sites, different *c*-BC_2N structures can be constructed with a cubic or noncubic shape of unit cells. Because of this, more parameters are needed to classify the crystal structures. We separate the BC_2N alloy into two categories, one without the high-energy B–B or N–N bonds and the other containing B–B, N–N, or both bonds. Consistent with previous calculations,[17,18] we find that structures with B–B or N–N bonds are highly unstable and have large volume relative to the structures without these bonds. In some cases, the N–N and B–B bonds break, which makes the structure seriously deformed from the diamond structure, so they are less likely to exist in the synthesized samples with high density.[8,9,11,12] In this study, we will focus mainly on the systems that do not have the unstable B–B and N–N bonds. In this case, we introduce a bond-type parameter η to describe the fraction of the ideal C–C and B–N bonds relative to the total number of the bonds, that is

$$\eta = \frac{n_{\mathrm{C-C}} + n_{\mathrm{B-N}}}{n_{\mathrm{C-C}} + n_{\mathrm{B-N}} + n_{\mathrm{C-B}} + n_{\mathrm{C-N}}}, \tag{1}$$

where *n* stands for the number of a specific bond in the structure. For the three $BC_2N_{1\times1}$ [Fig. 1(a)], $BC_2N_{2\times2}$, and $BC_2N_{3\times3}$ (111) superlattices, the bond number ratio of C–C:B–N:C–B:C–N are 3:3:1:1, 7:7:1:1, and 11:11:1:1, respectively, so η equals 0.75, 0.875, and 0.967, respectively. For the extensively studied BC_2N-*m* systems,[18,19,23,43] both BC_2N-1 and BC_2N-2 have $\eta=0.5$, whereas for BC_2N-3, $\eta=0$. Another structure studied here is the chalcopyrite struc-

TABLE II. Calculated alloy formation energy ΔE, lattice constants a_0, LDA-corrected lattice constants a_{th}, bulk moduli B_0, LDA-corrected bulk moduli B_{th}, the pressure derivative of bulk modulus B', and isotropic shear moduli G for diamond, c-BN, BC_2N structures studied in this paper, and $BC_4N_{2\times1}$ as function of alloy concentration x and bond-type parameter η. The LDA-corrected lattice constant results a_{th} can be compared with experimental values for BC_2N and BC_4N listed in Table I. The isotropic shear moduli G are also calculated using Eq. (4) from the calculated elastic constants reported in Ref. 18 for diamond, c-BN, BC_2N-1, BC_2N-2, and BC_2N-3, and in Ref. 44 for ch-BC_2N.

Structure	x	η	ΔE (eV/four atoms)	a_0 (Å)	a_{th} (Å)	B_0 (GPa)	B_{th} (GPa)	B'	G (GPa)
Diamond	1	1		3.542	3.567	454	421	3.56	539(547[a])
c-BN	0	1		3.593	3.616	392	364	3.81	405(407[a])
$BC_2N_{3\times3}$	0.5	0.967	0.39	3.573	3.597	422	393	3.53	449
$BC_2N_{2\times2}$	0.5	0.875	0.52	3.575	3.599	420	393	3.33	458
$BC_2N_{1\times1}$	0.5	0.750	0.76	3.579	3.603	420	390	3.70	458
BC_2N-1	0.5	0.500	1.78	3.586	3.610	398	374	3.15	431[a]
BC_2N-2	0.5	0.500	1.80	3.586	3.610	400	371	3.71	422[a]
r-BC_2N	0.5	0.250	2.62	3.602	3.626	382	358	3.20	
ch-BC_2N	0.5	0.000	3.41	3.607	3.631	377	348	4.06	436[b]
BC_2N-3	0.5	0.000	3.66	3.609	3.633	370	343	3.77	420[a]
$BC_4N_{2\times1}$	0.667	0.833	0.57	3.567	3.591	428	400	3.39	481

[a]Reference 18.
[b]Reference 44.

ture ch-BC_2N,[44] where the B and N atoms form a (201) superlattice in one of the fcc sublattices and C occupies the other sublattice. Similar to the BC_2N-3 structure, which is a (100) superlattice, it has no C–C and B–N bonds; thus, $\eta=0$. We have also included the r-BC_2N structure, which has $\eta=0.25$ and is randomly selected out of the 16-atom unit cell structures shown in Fig. 1(b). We also extend the $(C_2)_n/(BN)_n$ (111) superlattice model to the case of BC_4N, which can be taken as an alternative two-layer of the C_2 and one-layer of the BN superlattice along the (111) direction, denoted as $BC_4N_{2\times1}$ in Fig. 1(c).

Intuitively, one would expect that structures with large η should be more stable. This is the basis of the bond counting rule, which was proposed in the past to search for the low-energy BC_2N structures.[6,7,17,25] Using this bond counting rule, we have performed an unconstrained search (i.e., not limited by the shape of the primitive cell) for the low-energy BC_2N structure and identified $BC_2N_{1\times1}$ [Fig. 1(a)] as the lowest-energy structure with a 4-atom unit cell, $BC_2N_{2\times2}$ as the lowest-energy structure with an 8-atom unit cell, and $BC_2N_{3\times3}$ as the lowest-energy structure with a 12-atom unit cell. It will be shown subsequently in this paper that the intuition and the bond counting rule is correct.

B. Formation energy, lattice constant, and bulk modulus

For the alloy $(C_2)_x(BN)_{1-x}$ ($x=0.5$ for BC_2N, and $x=\frac{2}{3}$ for BC_4N), the formation energy is given by

$$\Delta E = E[(C_2)_x(BN)_{1-x}] - xE(C_2) - (1-x)E(BN), \quad (2)$$

where $E(C_2)$, $E(BN)$, and $E((C_2)_x(BN)_{1-x})$ stand for the calculated total energies per formula for diamond, c-BN, and $(C_2)_x(BN)_{1-x}$. The formation energies ΔE of a series of BC_2N structures are listed in Table II, from which we can see clearly that the formation energy decreases as η increases. If we plot the formation energy as a function of η, we can see that the dependence is almost linear [Fig. 2(a)], indicating that the formation energy decreases when the C–C and B–N bond numbers increase. The linear relation also indicates that the formation energy depends mainly on the bond type and is not sensitive to the specific atomic configu-

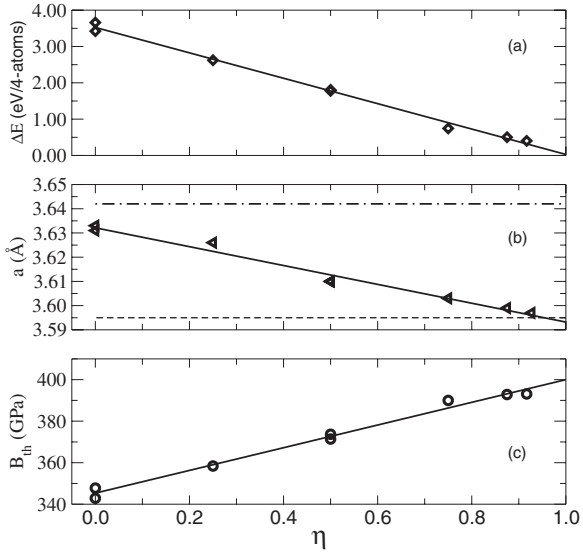

FIG. 2. Plot of calculated formation energy, LDA-corrected lattice constant, and bulk modulus as functions of the bond-type parameter η. The solid lines in each subfigure are linear fits of the calculated points, and the dashed line and dot-dashed line in (b) show the experimental lattice constants of BC_2N obtained by Zhao *et al.* (Ref. 11) for the high-density phase and by Solozhenko *et al.* (Ref. 10) for the low-density phase, respectively.

ration. This validates the bond counting rule used in the structure search.

The calculated lattice constants a_0 and LDA-corrected lattice constants a_{th} for the structures studied in this paper are listed in Table II. a_{th} is obtained in the following two steps: First, we use the relation $a_0^3 = V_{LDA}$, where V_{LDA} is the LDA-calculated equilibrium volume per eight atoms. Second, because LDA underestimates the calculated lattice constant for diamond and c-BN by 0.025 and 0.023 Å, respectively, to facilitate a direct comparison with experimental data, we have corrected the LDA error in the lattice constant by using the formula $a_{th}(x) = a_0 + 0.025x + 0.023(1-x)$. The LDA-corrected lattice constants of different BC_2N structures are plotted as a function of η in Fig. 2(b). The experimental value of Zhao *et al.*[11] for high-density BC_2N is shown as a dashed line, whereas the value of low density BC_2N produced by Solozhenko *et al.*[10] is shown as a dot-dashed line.

We find that the calculated lattice constants of BC_2N structures also decrease as η increases. The reason for the decrease in lattice constant caused by more C–C and B–N bonds is that the stable C–C and B–N bonds are shorter than the less stable C–B and C–N bonds as a whole. Once the number of B–N and C–C bonds increases while that of C–B and C–N bonds decreases, the average bond length and thus the lattice constant become smaller.

Comparing with experimental data, we see that the lattice constant measured by Zhao *et al.*[11] for the BC_2N structure is close to that for $\eta=1$; i.e., the $BC_2N_{n\times n}$ superlattices have lattice constants that are the closest to the experimental value with the deviation of less than 0.01 Å. According to this linear relationship between the lattice constant and η, the high-density sample obtained by Zhao *et al.*[11] should contain much more C–C and B–N bonds than C–B and C–N bonds. Therefore, the BC_2N-1, BC_2N-2, and other structures, which contain only 50% or less C–C and B–N bonds, may not be a good representation of the experimentally observed structures.[11] The calculated lattice constant of the $BC_4N_{2\times1}$ superlattice is also quite close to the experimental value, with a deviation of only 0.006 Å. Considering the good agreement between the lattice constants of (111) superlattices and the experimental values for BC_2N and BC_4N by Zhao *et al.*, we believe that the synthesized high-density sample may contain a large amount of (111) superlattices.

On the other hand, the calculated lattice constants for BC_2N structures without B–B and N–N bonds are all smaller than the experimental value of samples obtained by Solozhenko *et al.*,[10] even for $\eta=0$ [Fig. 2(b)]. Therefore, we suspect that the samples grown by Solozhenko *et al.* at very high temperature may contain significant amounts of unstable N–N and B–B bonds.

By fitting the total energy as a function of the volume near the equilibrium state to Murnaghan's equation of state (EOS), we calculate the bulk moduli for the structures listed in Table I. Because the LDA slightly underestimated the equilibrium volume, the calculated bulk moduli B_0 are systematically overestimated. To correct this error, we have used the definition of Murnaghan's EOS, i.e.,

$$B(V) = B_0 + B' P(V), \tag{3}$$

and calculated the bulk moduli at the LDA-corrected lattice constants. The results are shown in Table II and plotted in Fig. 2(c). We see that for all BC_2N structures studied here, the bulk moduli increase monotonically with η. This is consistent with the fact that the volume decreases monotonically with η. This is because when there are more C–C and B–N bonds in the BC_2N structure, it becomes denser and the strong bonds give a relatively high resistance to the volume change and, therefore, a larger bulk modulus. The predicted bulk moduli are all larger than the small bulk moduli observed in the samples grown by Solozhenko *et al.*, which is another strong indication that their sample may contain significant amounts of N–N and B–B bonds. However, previous studies[18,23] have shown that structures containing the unstable N–N and B–B bonds are usually weak with small elastic moduli and ideal strength; therefore, it is not clear if the measured high hardness of the low-density BC_2N sample[10] is its intrinsic property or not.

C. Isotropic shear modulus

Because the shear modulus is considered a better predictor of hardness than bulk modulus,[4] we also calculated the isotropic shear modulus of $BC_2N_{n\times n}$ superlattices. The isotropic shear modulus can be expressed by means of elastic constants in Voigt notation,[28,45]

$$G = \frac{1}{15}[(C_{11}+C_{22}+C_{33}) - (C_{23}+C_{31}+C_{12}) + 3(C_{44}+C_{55} + C_{66})], \tag{4}$$

where C_{ij} are elastic constants and can be estimated from first-principles calculation through fitting the total energy under small strains to a second-order Taylor expansion of the total energy as a function of strain.[7,46,47] If we take a hexagonal supercell for the rhombohedral or trigonal $BC_2N_{n\times n}$ (111) superlattices, setting the c axis along the (111) direction, then the number of independent elastic constants included in Eq. (4) reduces to 5, i.e., C_{11}, C_{12}, C_{13}, C_{33}, and C_{44}.[47] The isotropic shear modulus for a hexagonal cell is then expressed as

$$G = \frac{1}{15}\left(\frac{7}{2}C_{11} + C_{33} + 6C_{44} - \frac{5}{2}C_{12} - 2C_{13}\right). \tag{5}$$

Similar to the isotropic shear modulus, the bulk modulus can also be expressed as a function of elastic constants,[47]

$$B = \frac{2}{9}\left(C_{11} + C_{12} + 2C_{13} + \frac{1}{2}C_{33}\right). \tag{6}$$

To compare with the results of the $BC_2N_{n\times n}$ superlattices, we also calculate the elastic constants of diamond and c-BN using the hexagonal supercells with the c axis along the (111) direction. The calculated B from elastic constants (Table III) are slightly smaller than the one B_0 obtained by the directly fitting to Murnaghan's EOS (Table II). As Table III shows, the obtained isotropic shear moduli of diamond and c-BN agree quite well with the experimental values (Table I), indicating a high accuracy of our elastic constant calculation. The isotropic shear moduli of $BC_2N_{n\times n}$ all lie in between the values of c-BN and diamond, indicating that

TABLE III. Hexagonal elastic constants, the bulk moduli B, and the isotropic shear moduli G (in GPa) calculated from elastic constants of c-BN, diamond, $BC_2N_{n\times n}$, and $BC_4N_{2\times 1}$. For direct comparison with $BC_2N_{n\times n}$ and $BC_4N_{2\times 1}$, we calculate the elastic constants of diamond and c-BN in a hexagonal supercell with the c axis along the (111) direction.

Structure	C_{11}	C_{12}	C_{13}	C_{33}	C_{44}	B	G
Diamond	1176.92	87.66	60.62	1203.96	517.59	441.73	539.22
c-BN	942.09	117.16	78.69	980.56	373.99	379.31	404.77
$BC_2N_{1\times 1}$	1054.61	97.16	62.57	1041.40	417.70	399.47	458.05
$BC_2N_{2\times 2}$	1042.87	95.63	68.29	1081.08	419.78	403.16	458.28
$BC_2N_{3\times 3}$	1023.26	112.46	69.06	1098.78	412.59	405.16	449.10
$BC_4N_{2\times 1}$	1088.30	90.77	64.19	1103.00	444.20	413.10	481.46

$BC_2N_{n\times n}$ superlattices have a large resistance to various kinds of small elastic strains, above that of c-BN while below that of diamond.

Elastic constants of BC_2N-1, BC_2N-2, BC_2N-3, and chalcopyrite ch-BC_2N have previously been calculated,[18,44] from which we can deduce the isotropic shear moduli of these structures according to Eq. (4) (also shown in Table II). Since the bulk moduli B_0 calculated by us are close to the ones in these references, we believe that the isotropic shear moduli calculated from their elastic constants are comparable to our results, and actually the values of diamond and c-BN calculated from the elastic constants of Sun *et al.*[18] are 547 and 407 GPa, respectively, quite close to our results of 539 and 405 GPa. Comparing the isotropic shear modulus of $BC_2N_{n\times n}$, BC_2N-1, BC_2N-2, BC_2N-3, and ch-BC_2N, we find that $BC_2N_{n\times n}$ shows a higher resistance to elastic distortions among all proposed BC_2N structures.

Figure 3 plots the Vickers hardness of diamond, c-BN, BC_2N, and BC_4N samples measured by Zhao *et al.*[11] as a function of the calculated isotropic shear moduli. The points (solid circle) of diamond, c-BN, $BC_2N_{n\times n}$, and $BC_4N_{2\times 1}$ (111) superlattices fall almost on a straight line, showing that these superlattices should dominate the synthesized BC_2N and BC_4N samples if we accept that Vickers hardness relates linearly to the isotropic shear modulus, as Teter proposed.[4] What is more, this linear relationship also gives a reasonable explanation for the measured extreme hardness since these superlattices have a strong resistance to elastic deformation. We also show in Fig. 3 the points (hollow diamond points) corresponding to BC_2N-1, BC_2N-2, and ch-BC_2N that have fewer C–C and B–N bonds, and thus higher formation energy and larger volume. These three points significantly deviate from the hardness-G line, showing that if these high-energy structures dominate the BC_2N sample, then the measured hardness should be smaller according to Teter's correlation.

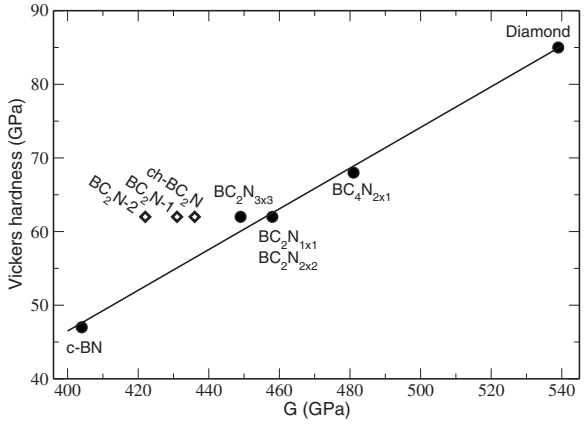

FIG. 3. Plot of the Vickers hardness measured by Zhao *et al.* for their synthesized diamond, c-BN, BC_2N, and BC_4N samples (Ref. 11) as a function of the calculated isotropic shear modulus for diamond, c-BN, different BC_2N, and BC_4N structures. We show that the data of diamond, c-BN, $BC_2N_{n\times n}$, and $BC_4N_{2\times 1}$ (solid circles) almost fall on a straight line, whereas BC_2N-1, BC_2N-2, and ch-BC_2N (hollow diamond points) do not fall on the same line.

D. Ideal strength and ideal shear strength under normal compression

The bulk modulus and isotropic shear modulus show the resistance to small volume deformation and elastic distortion. However, the material is seriously deformed in hardness measurement, so the ideal strength, the stress at which a perfect crystal becomes mechanically unstable,[23,41,48] was recently proposed by Zhang *et al.* to better reflect how the material responds under the large deformation.[23] Following their approach, we calculate the ideal tensile and shear strength for the short-period (111) superlattices $BC_2N_{1\times 1}$ and $BC_4N_{2\times 1}$, as well as diamond and c-BN [Figs. 4(a) and 4(b)]. Our calculations show that for both $BC_2N_{1\times 1}$ and $BC_4N_{2\times 1}$, the (111) direction is the weakest direction along which the minimum tensile stress can be sustained, and in the (111) plane the minimum shear stress can be sustained along the $[11\bar{2}]$ direction, which is the same as in diamond and c-BN. This is also why the diamond structure is amenable to the (111) cleavage.[49] Our calculated ideal tensile strength and ideal shear strength of diamond is 90.8 and 94.4 GPa, respectively, which is in good agreement with previous calculations.[23,41,49,50] The ideal tensile strengths for $BC_4N_{2\times 1}$, $BC_2N_{1\times 1}$, and c-BN are 79.3, 68.4, and 65.2 GPa, respectively, and ideal shear strengths are 64.9, 65.6, and 62.0 GPa (Ref. 25) (Table IV). Compared to the measured Vickers hardness for diamond, BC_4N, BC_2N, and c-BN of 85, 68, 62, and 47 GPa, respectively, the ideal tensile strengths are in the same trend as Vickers hardness, but the

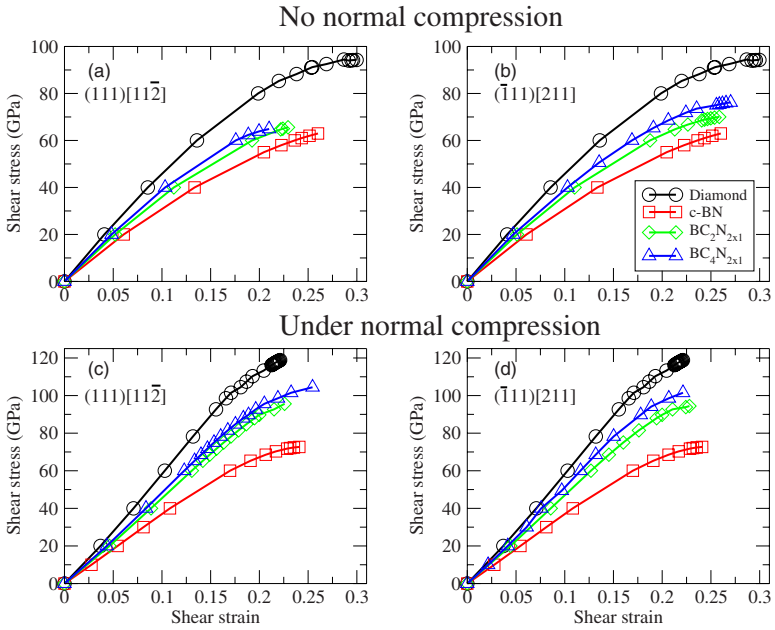

FIG. 4. (Color online) Plot of the calculated (111)[11$\bar{2}$] and ($\bar{1}$11)[211] shear stress without and with a normal compression as a function of shear strain for diamond, *c*-BN, $BC_2N_{1\times1}$, and $BC_4N_{2\times1}$. When the normal compression is applied, it equals to tan(68°) times the shear stress.

ideal shear strengths do not change monotonically with the Vickers hardness. Therefore, one should be cautious about using the ideal strength to infer the hardness, because the ideal strength reflects how well the material can sustain the strain along a single direction, whereas in hardness measurements, large strains along several directions are applied simultaneously under the indenter.

Recently, Pan *et al.* proposed to infer hardness from the shear strength under normal compression.[24] They think that the stress under the indenter contains a pure shear component and a normal compressive stress component that can reach tens or even thousands of gigapascals,[51–53] and the shear component σ_{yz} and normal compressive component σ_{zz} are related by $\sigma_{zz}/\sigma_{yz}=\tan\theta$, where θ is the centerline-to-face angle of the indenter. Since the Vickers, Knoop, and Berkovich indenters used in the hardness measurement all have similarly large centerline-to-face angles, they proposed to use the Vickers indenter value of $\theta=68°$. Following their approach, we calculate the ideal shear strength under normal compression for $BC_2N_{1\times1}$ and $BC_4N_{2\times1}$ [Figs. 4(c) and 4(d)] to compare with Vickers hardness measurement of high-density BC_2N and BC_4N from Zhao *et al.*

As we mentioned above, the diamond structure is easy to slip in the (111) plane along the [11$\bar{2}$] direction, and there are two nonequivalent (111) planes for $BC_2N_{1\times1}$ and $BC_4N_{2\times1}$: (111) and ($\bar{1}$11) planes; so, differing from the calculation of Pan *et al.* in which the shear strength was considered only in one of the (111) planes,[24] we consider here the shear strength in all nonequivalent (111) planes under normal compression. When there's no normal compression, the weakest direction for the shear stress of $BC_2N_{1\times1}$ is the [11$\bar{2}$] direction in the (111) plane, named (111)[11$\bar{2}$], and the value is 65.6 GPa, lower than 70.0 GPa along the nonequivalent ($\bar{1}$11)[211] direction (Table IV). When there is a normal compression, the shear strength along the (111)[11$\bar{2}$] direction increases to 95.6 GPa, slightly higher than the value 94.4 GPa along ($\bar{1}$11)[211]; therefore, ($\bar{1}$11)[211] becomes the weakest direction and the ideal shear strength under compression is 94.4 GPa. Similarly, for $BC_4N_{2\times1}$, the ($\bar{1}$11)[211] becomes the weakest direction under normal compression, with the shear strength equal to 101.5 GPa.

The calculated ideal shear strengths under normal compression are listed in Table IV, together with the values without compression for diamond, $BC_4N_{2\times1}$, $BC_2N_{1\times1}$, and *c*-BN. From these data, we can find that all calculated ideal shear strengths under normal compression have a significant enhancement relative to the corresponding values without compression, especially for diamond, $BC_4N_{2\times1}$, and $BC_2N_{1\times1}$, with the enhancement of more than 20 GPa. It is

TABLE IV. Calculated shear strength (in GPa) without and with normal compression in different (111) planes for diamond, *c*-BN, $BC_2N_{1\times1}$, and $BC_4N_{2\times1}$. When the normal compression is applied, it equals to tan(68°) times the shear stress.

Structure	Diamond	$BC_4N_{2\times1}$	$BC_4N_{2\times1}$	$BC_2N_{1\times1}$	$BC_2N_{1\times1}$	*c*-BN
Plane	(111)	(111)	($\bar{1}$11)	(111)	($\bar{1}$11)	(111)
Without normal compression	94.4	64.9	76.2	65.6	70.0	62.0(70.4[a])
Under normal compression	118.9	104.4	101.5	95.6	94.4	72.7(64.3[a])

[a]Reference 24.

important to note that in the calculation of Pan *et al.*,[24] the ideal strength decreases from 70.4 to 64.3 GPa for *c*-BN when a normal compression is applied, but from our calculation, it increases from 62.0 to 72.7 GPa. We also performed a test calculation on the $(111)[11\bar{2}]$ shear strength of diamond under a fixed 50 GPa normal compression. The result is 104.7 GPa, close to 108 GPa obtained by Chacham and Kleinman.[50] We think that the different trends for *c*-BN between the calculation of Pan *et al.* and our calculation should be due to the different relaxation processes for the structure with specific shear and compression stress targets. In our calculation, the structure is relaxed simultaneously in both normal and shear directions, whereas in the calculation of Pan *et al.*, a shear strain is applied first, and after determining the shear stress, the structure is relaxed to a target normal compression stress by fixing the shear strain and assuming the shear stress is also fixed. This could introduce error because under large deformation, the stresses along orthogonal directions are not independent of each other.

When the measured Vickers hardness[11] of diamond, *c*-BN, BC_2N, and BC_4N are plotted as a function of the calculated ideal shear strength under normal compression of diamond, *c*-BN, $BC_2N_{1\times1}$, and $BC_4N_{2\times1}$ (Fig. 5), we find that the ideal shear strength under normal compression also changes almost linearly with the Vickers hardness, like the isotropic shear modulus, indicating that the ideal shear strength under normal compression is a better predictor of hardness relative to the one without normal compression. The large ideal shear strengths under normal compression of BC_2N and BC_4N also explain the high hardness of the synthesized sample because these low-energy $BC_2N_{1\times1}$ and $BC_4N_{2\times1}$ superlattices can sustain a very large plastic distortion under indentation, together with a high resistance to small elastic distortion.

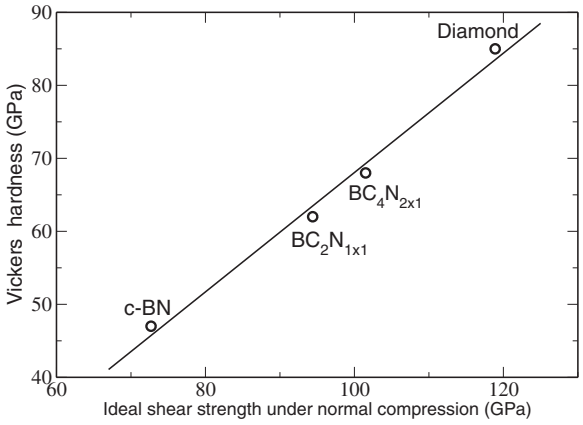

FIG. 5. Plot of the Vickers hardness measured by Zhao *et al.* for their synthesized diamond, *c*-BN, BC_2N, and BC_4N samples (Ref. 11) as a function of the calculated ideal shear strength under normal compression for diamond, *c*-BN, $BC_2N_{1\times1}$, and $BC_4N_{2\times1}$ superlattices.

IV. CONCLUSION

In summary, using first-principles calculations, we have studied the structural and elastic properties of the *c*-BN/C_2 alloy systems. We show that there is a sublinear dependence of the physical properties of *c*-BC_2N alloys on the number of C–C and B–N bonds in the structure. Structures that maximize the number of C–C and B–N bonds have low energy, high density, and high bulk and shear moduli. We also show that the low-energy $(C_2)_n/(BN)_m$ (111) superlattices have structural parameters similar to the recently synthesized high-density BC_2N and BC_4N samples. The calculated bulk and shear moduli and ideal shear strength under normal compression indicate that these (111) superlattices are very strong in resistance to elastic distortion at equilibrium and plastic distortion under nanoindentation. Furthermore, we find that the calculated shear moduli and ideal shear strength under normal compression relate linearly with the measured hardness and could thus be used as good indicators to predict the hardness of these alloys.

ACKNOWLEDGMENTS

The work at Fudan University is partially supported by the National Science Foundation of China, the Special Funds for Major State Basic Research, and the Shanghai Project. The computation is performed in the Supercomputer Center of Shanghai, the Supercomputer Center of Fudan University, and CCS. The work at NREL is funded by the U.S. Department of Energy under Contract No. DE-AC36-99GO10337.

[1] A. Zerr, G. Miehe, G. Serghiou, M. Schwarz, E. Kroke, R. Riedel, H. Fueβ, P. Kroll, and R. Boehler, Nature (London) **400**, 340 (1999).
[2] L. S. Dubrovinsky, N. A. Dubrovinskaia, V. Swamy, J. Muscat, N. M. Harrison, R. Ahuja, B. Holm, and B. Johansson, Nature (London) **410**, 653 (2001).
[3] M. L. Cohen, Science **261**, 307 (1993).
[4] D. M. Teter, Mater. Res. Bull. **23**, 22 (1998).
[5] R. B. Kaner, J. J. Gilman, and S. H. Tolbert, Science **308**, 1268 (2005).
[6] Y. Tateyama, T. Ogitsu, K. Kusakabe, S. Tsuneyuki, and S. Itoh, Phys. Rev. B **55**, R10161 (1997).
[7] M. Mattesini and S. F. Matar, Int. J. Inorg. Mater. **3**, 943 (2001).
[8] E. Knittle, R. B. Kaner, R. Jeanloz, and M. L. Cohen, Phys. Rev. B **51**, 12149 (1995).
[9] T. Komatsu, M. Samedima, T. Awano, Y. Kakadate, and S. Fujiwara, J. Mater. Process. Technol. **85**, 69 (1999).
[10] V. L. Solozhenko, D. Andrault, G. Fiquet, M. Mezouar, and D. C. Rubie, Appl. Phys. Lett. **78**, 1385 (2001).
[11] Y. Zhao, D. W. He, L. L. Daemen, T. D. Shen, R. B. Schwarz, Y. Zhu, D. L. Bish, J. Huang, J. Zhang, G. Shen, J. Qian, and T. W. Zerda, J. Mater. Res. **17**, 3139 (2002).

[12] W. Utsumi, S. Nakano, K. Kimoto, T. Okada, M. Isshiki, T. Taniguchi, K. Funakoshi, M. Akaishi, and O. Shimomura, Proceedings of AIRAPT-18, Beijing, China, 2001 (unpublished), p. 186.
[13] V. L. Solozhenko, S. N. Dub, and N. V. Novikov, Diamond Relat. Mater. **10**, 2228 (2001).
[14] L. Vegard, Z. Phys. **5**, 17 (1921).
[15] R. Q. Zhang, K. S. Chan, H. F. Cheung, and S. T. Lee, Appl. Phys. Lett. **75**, 2259 (1999).
[16] W. R. L. Lambrecht and B. Segall, Phys. Rev. B **40**, 9909 (1989).
[17] W. R. L. Lambrecht and B. Segall, Phys. Rev. B **47**, 9289 (1993).
[18] H. Sun, S. H. Jhi, D. Roundy, M. L. Cohen, and S. G. Louie, Phys. Rev. B **64**, 094108 (2001).
[19] E. Kim, T. Pang, W. Utsumi, V. L. Solozhenko, and Y. Zhao, Phys. Rev. B **75**, 184115 (2007).
[20] In Ref. 19, the bulk moduli are calculated using the elastic constants, instead of fitting to the Murnaghan EOS. This procedure usually underestimates the bulk moduli. In Ref. 21, the calculated GGA lattice constants for diamond and *c*-BN are much smaller than the experimental values (Table I) and GGA values in a previous calculation.
[21] A. Janotti, S.-H. Wei, and D. J. Singh, Phys. Rev. B **64**, 174107 (2001).
[22] X.-F. Zhou, J. Sun, Y.-X. Fan, J. Chen, H.-T. Wang, X. Guo, J. He, and Y. Tian, Phys. Rev. B **76**, 100101(R) (2007).
[23] Y. Zhang, H. Sun, and C. Chen, Phys. Rev. Lett. **93**, 195504 (2004).
[24] Z. Pan, H. Sun, and C. Chen, Phys. Rev. Lett. **98**, 135505 (2007).
[25] S. Chen, X. G. Gong, and S.-H. Wei, Phys. Rev. Lett. **98**, 015502 (2007).
[26] S. Chen, X. G. Gong, and S.-H. Wei, Phys. Rev. Lett. **99**, 159602 (2007).
[27] C. Chen and H. Sun, Phys. Rev. Lett. **99**, 159601 (2007).
[28] M. Mattesini and S. F. Matar, Comput. Mater. Sci. **20**, 107 (2001).
[29] X. Luo, X. Guo, B. Xu, Q. Wu, Q. Hu, Z. Liu, J. He, D. Yu, Y. Tian, and H. T. Wang, Phys. Rev. B **76**, 094103 (2007).
[30] C. Kittel, *Introduction to Solid State Physics*, 7th ed. (Wiley, New York, 1996), p. 92.
[31] E. Knittle, R. M. Wentzcovitch, R. Jeanloz, and M. L. Cohen, Nature (London) **337**, 349 (1989).
[32] M. Grimsditch, E. S. Zouboulis, and A. Polian, J. Appl. Phys. **76**, 832 (1994).
[33] S. N. Tkachev, V. L. Solozhenko, P. V. Zinin, M. H. Manghnani, and L. C. Ming, Phys. Rev. B **68**, 052104 (2003).
[34] X. Gonze, J.-M. Beuken, R. Caracas, F. Detraux, M. Fuchs, G.-M. Rignanese, L. Sindic, M. Verstraete, G. Zerah, F. Jollet, M. Torrent, A. Roy, M. Mikami, Ph. Ghosez, J.-Y. Raty, and D. C. Allan, Comput. Mater. Sci. **25**, 478 (2002).
[35] X. Gonze, G.-M. Rignanese, M. Verstraete, J.-M. Beuken, Y. Pouillon, R. Caracas, F. Jollet, M. Torrent, G. Zerah, M. Mikami, Ph. Ghosez, M. Veithen, J.-Y. Raty, V. Olevano, F. Bruneval, L. Reining, R. Godby, G. Onida, D. R. Hamann, and D. C. Allan, Z. Kristallogr. **220**, 558 (2005).
[36] N. Troullier and J. L. Martins, Phys. Rev. B **43**, 1993 (1991).
[37] S. Goedecker, M. Teter, and J. Hutter, Phys. Rev. B **54**, 1703 (1996).
[38] H. J. Monkhorst and J. D. Pack, Phys. Rev. B **13**, 5188 (1976).
[39] D. Roundy, C. R. Krenn, M. L. Cohen, and J. W. Morris, Phys. Rev. Lett. **82**, 2713 (1999).
[40] D. Roundy, C. R. Krenn, M. L. Cohen, and J. W. Morris, Philos. Mag. A **81**, 1725 (2001).
[41] D. Roundy and M. L. Cohen, Phys. Rev. B **64**, 212103 (2001).
[42] H. B. Schlegel, J. Comput. Chem. **3**, 214 (1982).
[43] Z. Pan, H. Sun, and C. Chen, Phys. Rev. B **70**, 174115 (2004).
[44] J. Sun, X.-F. Zhou, G.-R. Qian, J. Chen, Y.-X. Fan, H.-T. Wang, X. Guo, J. He, Z. Liu, and Y. Tian, Appl. Phys. Lett. **89**, 151911 (2006).
[45] A. Reuss, Z. Angew. Math. Mech. **9**, 49 (1929).
[46] P. Ravindran, L. Fast, P. A. Korzhavyi, B. Johansson, J. Wills, and O. Eriksson, J. Appl. Phys. **84**, 4891 (1998).
[47] S. Q. Wang and H. Q. Ye, J. Phys.: Condens. Matter **15**, 5307 (2003).
[48] G. Galli, F. Gygi, and A. Catellani, Phys. Rev. Lett. **82**, 3476 (1999).
[49] R. H. Telling, C. J. Pickard, M. C. Payne, and J. E. Field, Phys. Rev. Lett. **84**, 5160 (2000).
[50] H. Chacham and L. Kleinman, Phys. Rev. Lett. **85**, 4904 (2000).
[51] Y. G. Gogotsi, A. Kailer, and K. G. Nickel, Nature (London) **401**, 663 (1999).
[52] K. J. Van Vliet, J. Li, T. Zhu, S. Yip, and S. Suresh, Phys. Rev. B **67**, 104105 (2003).
[53] T. Zhu, J. Li, K. J. V. Vliet, S. Ogata, S. Yip, and S. Suresh, J. Mech. Phys. Solids **52**, 691 (2004).